Journal of Organometallic Chemistry, 409 (1991) 271–284
Elsevier Sequoia S.A., Lausanne
JOM 21639

Synthesis, molecular and electronic structure of $Os_3(CO)_{10}(\mu_2\text{-}\eta^3\text{-}C_3H_5)(AuPEt_3)$: a triosmium cluster exhibiting an allyl ligand with a novel mode of coordination

Catherine E. Housecroft *, Brian F.G. Johnson, Jack Lewis *, Julie A. Lunniss, Steven M. Owen and Paul R. Raithby

University Chemical Laboratory, Lensfield Road, Cambridge CB2 1EW (UK)

(Received December 6th, 1990)

Abstract

The synthesis and characterisation of a new triosmium cluster, $Os_3(CO)_{10}(\mu_2\text{-}\eta^3\text{-}C_3H_5)(AuPEt_3)$ (**1**) are reported. The cluster is formed most efficiently by the deprotonation of $HOs_3(CO)_{10}(HC{=}CHMe)$ followed by reaction with Et_3PAuCl, a step that stabilises the anion $[Os_3(CO)_{10}(\mu_2\text{-}\eta^3\text{-}C_3H_5)]^-$. This anion is also the product of the reaction between the cluster anion $[HOs_3(CO)_{11}]^-$ and 1-propyne. The molecular structure of **1** has been determined. The allylic moiety bridges one Os–Os edge of the triosmium triangular cluster core in a $\mu_2\text{-}\eta^3$ fashion. The electronic structure of **1** has been investigated by the Fenske–Hall quantum chemical technique; the results illustrate the primary involvement of the allyl non-bonding MO and have been used to suggest possible orientations for the allylic hydrogen atoms.

The development of a range of systematic syntheses of mono- and dinuclear transition metal allyl complexes has established them as an important and broadly studied class of organometallic compounds [1]. As metal-bound ligands, allyl groups are capable of acting as one-electron donors (σ-allyls) or as three-electron donors (π-allyls). In the latter mode of bonding, the π-allyl coordinates to either one or two metal atoms. Their capacity for facile and reversible changes in their bonding mode is well documented and lends them importance as intermediates in several homogeneous catalytic processes [2].

The interaction of organic molecules or molecular fragments with metallic centres is commonly encountered in transition metal cluster chemistry. However, in contrast to the mono- and dinuclear systems, there are relatively few examples of clusters which contain an allyl group [3–7]. In this paper, we report the synthesis of the novel allyl-containing cluster compound $Os_3(CO)_{10}(\mu_2\text{-}\eta^3\text{-}C_3H_5)(AuPEt_3)$ (**1**). A description of its molecular structure in the solid state and its solution ^1H NMR spectral properties are presented, along with a Fenske–Hall molecular orbital analysis of the bonding in **1**.

0022-328X/91/$03.50

Experimental

General

All operations were performed under a nitrogen atmosphere unless otherwise stated. Solvents were freshly dried and distilled. 1-Propyne was used directly without purification; DBU (1,8-diazabicyclo[5.4.0]undec-7-ene) was distilled prior to use. The compounds Et_3PAuCl [8] and $[PPN][HOs_3(CO)_{11}]$ [9] (PPN = bis-(triphenylphosphine)iminium(1 +)) were prepared by standard literature methods. Infrared and mass spectra were recorded on a Perkin–Elmer FT 1710 spectrophotometer and an AEI-MS-12 instrument respectively. ^1H NMR spectra were recorded on a Brüker WM 250 MHz spectrometer; chemical shifts are with respect to $\delta = 0$ ppm for Me_4Si and all downfield chemical shifts are positive. Preparative thin layer plate chromatography used Merck Kieselgel 60-F_{254}.

Reaction of $[PPN][HOs_3(CO)_{11}]$ with 1-propyne

1-Propyne was bubbled through a THF solution (25 mL) of $[PPN][HOs_3(CO)_{11}]$ (100 mg, 0.07 mmol) for several minutes. The flask was then sealed and over a period of 16 h, the solution changed in colour from red to orange. The addition of one equivalent of Et_3PAuCl produced a sight darkening of the solution. The reaction mixture was separated by TLC by eluting with CH_2Cl_2/hexanes (1/9). Four fractions were collected: band one (bright yellow, 10–20%, EI *m/z* P^+ 898) was $HOs_3(CO)_{10}(HCCHMe)$ (**2**) [10*]; band two (pale orange, 2% yield, EI *m/z* P^+ 1212) was identified as $Os_3(CO)_{10}(HCCHMe)(AuPEt_3)$ (**3**); band three (orange, 30–40% yield, EI *m/z* P^+ 1212) identified as $Os_3(CO)_{10}(MeCCH_2)(AuPEt_3)$ (**4**); band four (pale yellow, 10% yield, EI *m/z* P^+ 1212) proved to be $Os_3(CO)_{10}(\mu_2\text{-}\eta^3\text{-}C_3H_5)(AuPEt_3)$ (**1**).

Alternative route to 1

$HOs_3(CO)_{10}(HCCHMe)$ (**2**) [11*], (20 mg, 0.02 mmol) was dissolved in THF (20 mL) and was treated with one equivalent of DBU. The reaction was monitored with infrared spectroscopy and, after 10 min, Et_3PAuCl (slightly in excess of 1 mol equivalent) was added whereupon the colour of the solution changed from deep yellow to yellow-orange. The products were separated by TLC by eluting with CH_2Cl_2/hexanes (1/9). Three fractions were collected. The first band (yellow) was unreacted **2**; the second band (pale orange, 10% yield) was identified as $Os_3(CO)_{10}(HCCHMe)(AuPEt_3)$ (**3**); the third band (yellow, 40% yield) was compound **1**.

*Crystal structure determination of **1***

A suitable yellow, block-shaped crystal was obtained by slow evaporation from petroleum ether (40–60 °C boiling fraction) at 0 °C and was mounted on a glass fibre with epoxy resin.

Crystal data. $C_{19}H_{20}AuO_{10}POs_3$, $M = 1206.89$, triclinic, a 9.086(14), b 11.110(14), c 13.393(11) Å, α 90.34(8), β 99.47(9), γ 100.82(11)°, V 1309 Å^3, (by least-squares refinement on diffractometer angles from 44 automatically centred

* Reference number with asterisk indicates a note in the list of references.

reflections, 2θ range 20–25°, λ 0.71069 Å), space group $P\bar{1}$ (no. 2), Z 2, D_c 3.06 g cm^{-3}, $F(000) = 1072$. Yellow rectangular blocks. Crystal dimensions (distance to faces from centre): 0.093 (100, $\bar{1}00$) × 0.133 (010, $0\bar{1}0$) × 0.148 ($\bar{1}11$, $1\bar{1}\bar{1}$) × 0.106 (011, $0\bar{1}\bar{1}$) × 0.139 ($0\bar{1}1$, $01\bar{1}$) × 0.061 (001, $00\bar{1}$) mm, μ(Mo-K_α) 201.78 cm^{-1}.

Data collection and processing. Stoe-Siemens AED diffractometer, 24 step ω–θ mode with ω scan width 0.05° for each step, scan time 0.75–3.0 s per step, graphite monochromated Mo-K_α radiation. 3574 reflections measured ($5.0 \leqslant 2\theta \leqslant 45.0°$, $\pm h$, $\pm k$, $+l$), 3400 unique (merging R 0.025 after numerical absorption correction, maximum, minimum transmission factors 0.112, 0.013), giving 2499 with $F > 4\sigma(F)$. Three standard reflections showed no significant variation in intensity.

Structure analysis and refinement

Direct methods (Os and Au atoms) followed by Fourier difference techniques. Blocked full-matrix least-squares refinement with Os, Au, P and O atoms anisotropic. Hydrogen atoms not located. The weighting scheme $w = 1.80/[\sigma^2(F) + 0.001F_o^2]$ with $\sigma(F_o)$ from counting statistics gave satisfactory agreement analyses. Final converged R and R' values were 0.045 and 0.047. A final difference map showed peaks of ca. 1.8 e $Å^{-3}$ close to the positions of the metal atoms but no other regions of significant electron density. The structure was solved and refined by using SHELX76 [12] implemented on the University of Cambridge IBM 3084Q computer. Scattering factors were taken from ref. 13. Final atomic coordinates and equivalent displacement parameters are listed in Table 1. Details of the thermal parameters, complete lists of bond parameters, and structure factors may be obtained from the authors.

Molecular orbital calculations

Fenkse–Hall [14] calculations were carried out by using $Ru_3(CO)_{10}(C_3H_5)$-$(CuPH_3)$ [15*] and $[Ru_3(CO)_{10}(C_3H_5)]^-$ as models (see text) for $Os_3(CO)_{10}(C_3H_5)$-$(AuPEt_3)$. The molecular geometries for $Ru_3(CO)_{10}(C_3H_5)(CuPH_3)$ [15*] and $[Ru_3(CO)_{10}(C_3H_5)]^-$ were based on the experimentally determined structure for $Os_3(CO)_{10}(C_3H_5)(AuPEt_3)$. The geometry for the anion was idealised to C_s symmetry. All C–O bonds were set at 1.13 Å and Ru–CO bonds were 1.90 Å. Atomic numbering and the axis system for the calculations are shown in Scheme 1; in $[Ru_3(CO)_{10}(C_3H_5)]^-$, atoms Ru(1) and Ru(2) are symmetry related. Bond distances: Ru(1)–Ru(2) 2.94, Ru(1)–Ru(3) 2.85, Ru(1)–C(1) 2.19, Ru(1)–C(2) 2.58, C–H 1.08 Å. In $Ru_3(CO)_{10}(C_3H_5)(CuPH_3)$, Ru(1)–Cu 2.67, Ru(3)–Cu 2.74, Cu–P 2.21, P–H 1.41 Å.

The Fenske–Hall calculations employed single-ζ Slater functions for the 1*s* and 2*s* functions of C and O. The exponents were obtained by curve fitting the double-ζ functions of Clementi [16] while maintaining orthogonal functions; the double-ζ functions were used directly for the 2*p* orbitals. An exponent of 1.16 as used for hydrogen. The Ru functions [17] were augmented by 5*s* and 5*p* functions with exponents of 2.20.

Results and discussion

*The formation of **1**, **2**, **3** and **4***

The reaction of $[PPN][HOs_3(CO)_{11}]$ with 1-propyne and subsequent addition of Et_3PAuCl to the reaction mixture produces four cluster products. One exhibits an

Table 1

Atomic coordinates for $Os_3(CO)_{10}(C_3H_5)(AuPEt_3)$ (1)

Atom	x	y	z	U_{eq} [a]
Os(1)	11442(1)	1862(1)	Q757(1)	30(1)
Os(2)	8161(1)	999(1)	2121(1)	34(1)
Os(3)	9276(1)	3617(1)	2337(1)	32(1)
Au(1)	12455(1)	4355(1)	2822(1)	37(1)
P(1)	14114(6)	6185(5)	2917(4)	41(2)
C(11)	11789(24)	1915(18)	1345(16)	37(5)
O(11)	12130(21)	1952(16)	578(12)	65(7)
C(12)	13492(24)	2182(17)	3202(14)	33(5)
O(12)	14859(18)	2278(14)	3554(12)	57(6)
C(13)	11152(23)	1786(18)	4152(16)	36(5)
O(13)	11037(20)	1681(15)	4968(11)	59(7)
C(21)	8413(25)	1010(20)	712(17)	44(5)
O(21)	8388(22)	1012(14)	−145(13)	69(8)
C(22)	7871(23)	965(18)	3535(16)	35(5)
O(22)	7679(18)	929(16)	4318(12)	64(7)
C(23)	6061(28)	572(20)	1684(16)	48(6)
O(23)	4702(21)	388(17)	1456(16)	92(9)
C(31)	9184(24)	3557(19)	3779(16)	39(5)
O(31)	9179(19)	3617(14)	4595(11)	60(7)
C(32)	9722(22)	3631(17)	940(15)	34(5)
O(32)	9875(22)	3668(15)	159(12)	72(8)
C(33)	7109(25)	3366(19)	1933(15)	40(5)
O(33)	5836(17)	3405(15)	1688(12)	61(7)
C(34)	9733(26)	5327(21)	2420(16)	48(6)
O(34)	9816(22)	6436(14)	2458(15)	78(8)
C(1)	11546(25)	−111(20)	2769(16)	46(5)
C(2)	10049(35)	−387(27)	2097(22)	83(9)
C(3)	8603(27)	−861(21)	2220(17)	54(6)
C(111)	16155(24)	6163(19)	3185(15)	43(5)
C(112)	16568(25)	5544(20)	4219(16)	49(6)
C(121)	13764(24)	7301(19)	3854(15)	41(5)
C(122)	14866(26)	8523(21)	3976(16)	50(6)
C(131)	14002(31)	6992(24)	1709(20)	68(7)
C(132)	14119(39)	6241(30)	821(25)	98(10)

[a] Equivalent isotropic U defined as one third of the trace of the orthogonalized U_{ij} tensor.

allyl fragment and three are vinyl compounds. The vinyl clusters $HOs_3(CO)_{10}(HCCHMe)$ (2), $Os_3(CO)_{10}(HCCHMe)(AuPEt_3)$ (3) and $Os_3(CO)_{10}(MeCCH_2)(AuPEt_3)$ (4) were characterised on the basis of their mass and ^1H NMR spectral data. Presumably, the vinyl unit arises from the transfer of a hydrogen atom from the metal framework to the acetylene molecule. The observed yields of 3 (2%) and 4 (40%) suggest that the reaction of 1-propyne with $[HOs_3(CO)_{11}]^-$ occurs via a Markownikoff addition. The allyl cluster, 1, is formed in only a 10% yield but may be produced more efficiently by the deprotonation of 2 followed by reaction with Et_3PAuCl. Cluster 3 is produced as a minor product of this reaction. Spectroscopic data for compounds 1 to 4 are listed in Table 2. The room temperature ^1H NMR spectrum of 1 exhibited a complex set of resonances that suggested the presence of a π-allyl ligand. However, without knowledge of the exact mode of coordination, it

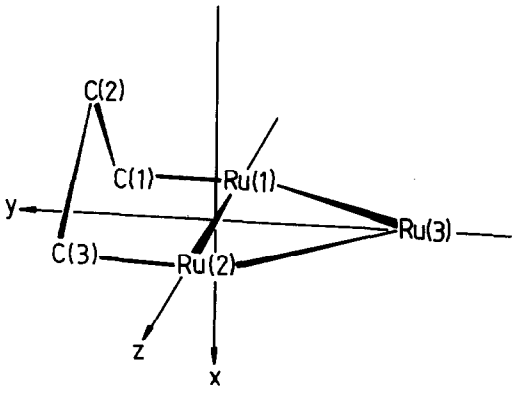

Scheme 1

was difficult to unambiguously assign the spectrum. The solid state structure of **1** was therefore determined.

Molecular structure of 1

The molecular structure of **1** is shown in Fig. 1 and selected bond lengths and angles are listed in Table 3. The triosmium core of **1** consists of a scalene triangle with Os(1)–Os(2) 2.935(1), Os(2)–Os(3) 2.890(1) and Os(1)–Os(3) 3.014(1) Å. The

Table 2

Selected spectroscopic data for compounds **1–4**

Complex	IR ν(CO) (cm^{-1}) [a]	NMR [b]			
		δ (ppm)	Relative intensity	Assignment [c]	J (Hz)
1	2076w, 2053s, 2034m,	3.42(ddd)	1	[d]	
	2025vs, 2016s, 1997ms,	3.32(ddd)	1	[d]	
	1987m, 1981m, 1971m,	2.69(m)	1	[d]	
	1948w	1.58(m)	15	Et	
		0.95(dd)	1	[d]	
		0.76(dd)	1	[d]	
2	2105w, 2079m, 2073m,	7.11(dd)	1	H_c	$J(H_cH_b) = 13.8$
	2060s, 2054s, 2021s	4.74(dq)	1	H_b	$J(H_bMe) = 5.7$
	2012s, 2004ms, 1996m	2.08(d)	3	Me	
	1980m	−18.79(d)	1	H_a	$J(H_aH_c) = 1.4$
3	2085w, 2054m, 2031s	7.26(d)	1	H_a	$J(H_aH_b) = 13.4$
	1996m, 1983w, 1958w	4.64(dq)	1	H_b	$J(H_bMe) = 5.6$
		1.66(m)	18	Me and Et	
4	2085m, 2054m, 2046w,	5.46(s)	1	H_b or H_d	
	2033vs, 2023s, 2004ms,	4.57(s)	1	H_d or H_b	
	1996s, 1985m, 1975m,	3.16(s)	3	Me	
	1964m, 1958m, 1946m	1.54(m)	15	Et	

[a] Recorded in cyclohexane solution. [b] Recorded in CD_2Cl_2 at 25 °C; s = singlet, d = doublet, q = quartet, m = multiplet. [c] For $H_aOs_3(CO)_{10}(CR^1CH_bR^2)$ or $Os_3(CO)_{10}(CR^1CH_bR^2)(AuPEt_3)$, $R^1 = H_c$ or Me, R^2 = Me or H_d. [d] See text.

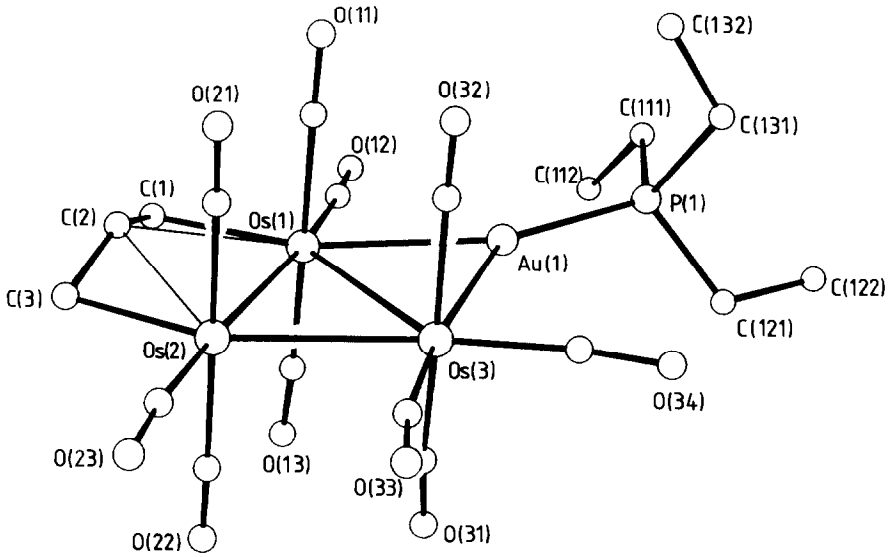

Fig. 1. Molecular structure of **1**.

longest Os–Os edge corresponds to that bridged by the $AuPEt_3$ group. Such bond lengthening is a common effect in clusters containing a μ-$AuPR_3$ unit [18] and may be attributed to the gold fragment using only its radial frontier MO in bonding to the cluster [19]. The $AuPEt_3$ group lies 0.18 Å out of the plane of the three osmium atoms such that the dihedral angle between the Os(1)Os(3)Os(2) and Os(1)Os(3)Au(1) planes is 4.3°. The bridge is asymmetric: Os(1)–Au(1) 2.736(1) compared to Os(3)–Au(1) 2.816(1) Å. There is nothing exceptional about the carbonyl ligands, all

Table 3

Selected bond lengths (Å) and angles (°) for **1**

Os(1)–Os(2)	2.935(1)	Os(1)–Os(3)	3.014(1)
Os(2)–Os(3)	2.890(1)	Os(1)–Au(1)	2.746(1)
Os(3)–Au(1)	2.816(1)	Os(1)–C(1)	2.209(22)
Os(1)–C(2)	2.654(27)	Os(2)–C(2)	2.514(34)
Os(2)–C(3)	2.177(24)	C(1)–C(2)	1.481(35)
C(2)–C(3)	1.359(39)	Au(1)–P(1)	2.281(5)
Os(3)–Os(1)–Os(2)	58.1(1)	Au(1)–Os(1)–Os(3)	58.3(1)
Au(1)–Os(3)–Os(1)	56.1(1)	Os(1)–Au(1)–Os(3)	65.6(1)
P(1)–Au(1)–Os(1)	159.0(2)	P(1)–Au(1)–Os(3)	135.0(2)
Os(2)–Os(3)–Os(1)	59.6(1)	Os(3)–Os(2)–Os(1)	62.3(1)
C(1)–Os(1)–Os(2)	84.6(6)	C(2)–Os(1)–Os(2)	53.2(7)
C(2)–Os(1)–C(1)	33.9(9)	Os(2)–C(3)–C(2)	87.4(17)
C(2)–Os(2)–Os(1)	57.7(6)	Os(1)–C(2)–Os(3)	122.5(21)
C(2)–Os(2)–C(3)	32.7(9)	Os(1)–C(1)–C(2)	89.7(16)
Os(2)–C(2)–Os(1)	69.2(8)	C(1)–C(2)–C(3)	135.4(26)
C(1)–C(2)–Os(1)	56.4(12)	C(1)–C(2)–Os(2)	120.5(18)
C(3)–C(2)–Os(1)	122.5(21)	C(3)–C(2)–Os(2)	59.9(16)
Os(2)–C(3)–C(2)	87.4(17)		

of which are in terminal positions. The edge Os(1)–Os(2) is bridged by an allyl group which is coordinated in an unusual μ_2-η^3 mode and formally contributed three electrons to the triosmium cluster. The internal dihedral angle between the planes defined by atoms C(1)C(2)C(3) and Os(1)Os(2)Os(3) is 76.2°, meaning that the central carbon atom, C(2), is significantly further from the two osmium atoms than are the peripheral carbon atoms, (2.65(3) and 2.51(3) Å compared to 2.21(2) and 2.18(2) Å). Note that the C_3-unit is slightly skewed with respect to the Os(1)–Os(2) edge. One other related cluster, $Ru_3(CO)_8(\mu_2\text{-}\eta^3\text{-}C_3H_5)(\mu_3\text{-}P(Ph)CH_2PPh_2)$ has been crystallographically characterised [5] and the metal–allyl distances observed here for **1** compare favorably with those reported for $Ru_3(CO)_8(\mu_2\text{-}\eta^3\text{-}C_3H_5)(\mu_3\text{-}P(Ph)CH_2PPh_2)$.

Electronic structure of 1

The aims of the Fenske–Hall quantum chemical studies were two-fold: (i) to provide a description of the bonding of the allyl fragment to the trimetal-framework, and (ii) to attempt to indirectly "locate" the allylic hydrogen atoms in **1**. In order to simplify the cluster bonding analysis, the anion $[Ru_3(CO)_{10}(C_3H_5)]^-$ was used as a model compound. The validity of this simplification was tested by comparing the results of calculations on $[Ru_3(CO)_{10}(C_3H_5)]^-$ and $Ru_3(CO)_{10}(C_3H_5)(CuPH_3)$, the latter being in terms of an $[Ru_3(CO)_{10}CuPH_3]^-/[C_3H_5]^+$ two fragment analysis. The results are summarised in Fig. 2. The $[CuPH_3]^+$ electrophile is, as expected [20], bonded in a localised manner to the metal framework. Comparison of the character of the complexed $[C_3H_5]^+$ ligand in $[Ru_3(CO)_{10}(C_3H_5)]^-$ and in $Ru_3(CO)_{10}(C_3H_5)(CuPH_3)$ indicates that the bonding mode of the allylic fragment is not significantly affected by the interaction of $[Ru_3(CO)_{10}(C_3H_5)]^-$ with the $[CuPH_3]^+$ fragment. For this reason, further discussion centres on the interactions of the $[Ru_3(CO)_{10}]^{2-}$ and $[C_3H_5]^+$ fragments to generate $[Ru_3(CO)_{10}(C_3H_5)]^-$.

Mode of bonding of the allyl ligand

The electronic structure of mononuclear transition metal-allyl complexes has been thoroughly documented [19]. In such complexes, the allyl ligand adopts a planar geometry, and the π-system of the ligand is perpendicular to the allyl-CCC plane. The frontier orbitals of the allyl ligand are shown schematically in Fig. 3. We began our investigation of the bonding in $[Ru_3(CO)_{10}(C_3H_5)]^-$ with the carbon atoms of the allyl fragment in experimentally determined, but idealised, positions, and the five hydrogen atoms coplanar with the carbon atoms. A correlation diagram for the interaction of the $[Ru_3(CO)_{10}]^{2-}$ and $[C_3H_5]^+$ fragments is shown in Fig. 3. The relative importance of each fragment–fragment orbital interaction is illustrated by the Mulliken overlap populations listed in Table 4. In line with previous observations [21], the primary interaction orbital of the allyl ligand is the non-bonding orbital, MO 9 (Fig. 3). Its interactions with MO's 60, 62 and 65 of the $[Ru_3(CO)_{10}]^{2-}$ fragment are represented in Fig. 4. Orbitals 8, (the HOMO), and 10 of $[C_3H_5]^+$ play a smaller part in binding the ligand to the metal fragment. The Mulliken populations of these orbitals (Table 5) change by small and approximately equal amounts: MO 8 loses 0.14 electrons and MO 10 gains 0.18 electrons. Both changes are consistent with a net decrease in carbon–carbon bonding character within the allyl ligand upon coordination. This is observed experimentally; the

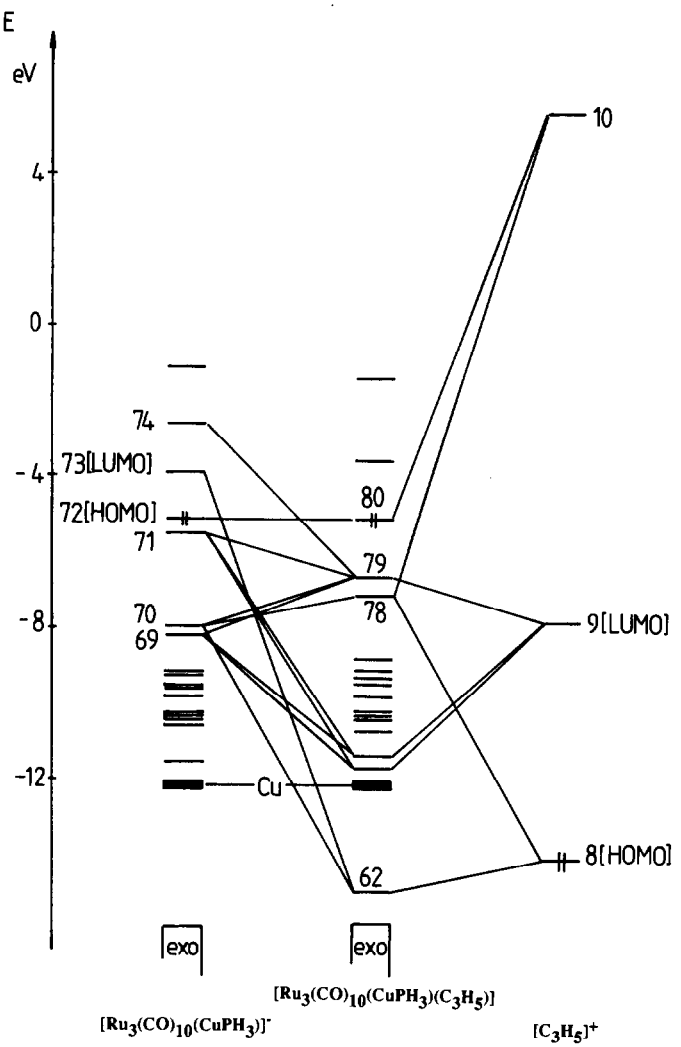

Fig. 2. Correlation diagram for the formation of the model compound $Ru_3(CO)_{10}(CuPH_3)(C_3H_5)$ from fragments $[C_3H_5]^+$ and $[Ru_3(CO)_{10}(CuPH_3)]^-$.

average allyl C–C bond length in **1** is 1.42 Å, compared to 1.39 Å for a typical C–C bond of bond order 1.5.

That the LUMO of the allyl ligand dominates the ligand–metal interactions, is borne out in the experimental orientation of the allyl unit with respect to the metal framework in **1**; viz. C(1) and C(3) are equidistant from Os(1) and Os(2) and lie in the plane of the metal triangle, while C(2) is significantly more remote from the metal atoms. Thus, despite there being more scope for multicentre bonding in a transition metal cluster vs. a mononuclear transition metal-allyl complex, and despite the allyl ligand in **1**, (and in the model $[Ru_3(CO)_{10}(C_3H_5)]^-$), interacting with two, and not just one, metal atoms, the primary involvement of the allyl non-bonding MO remains common to, and dominant in, both types of complex.

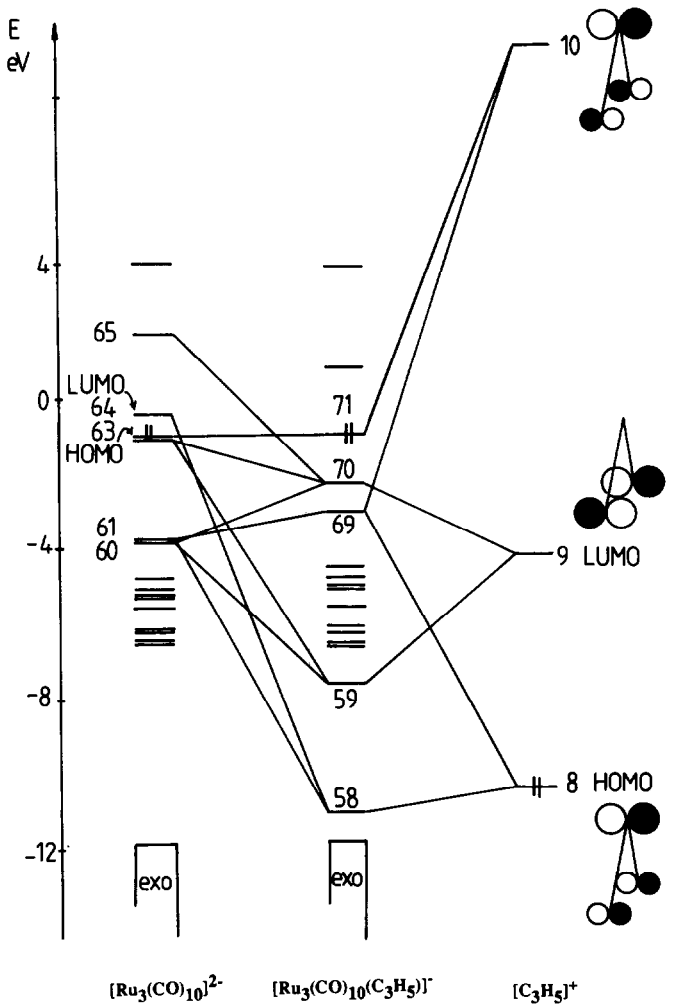

Fig. 3. Correlation diagram for the formation of the model anion $[Ru_3(CO)_{10}(C_3H_5)]^-$ from the fragments $[Ru_3(CO)_{10}]^{2-}$ and $[C_3H_5]^+$ and schematic representations of the frontier orbitals of the allyl ligand.

Hydrogen atom orientation in the allyl ligand

Since the hydrogen atoms in **1** were not located crystallographically, an initial assumption regarding ligand planarity was made. However, it is well established that organic π-ligands can optimise their interaction with metal fragments by reorientating the C–H bond vectors upon ligand complexation [22].

Repositioning the hydrogen atoms has the effect of redirecting not only the C–H σ-bonds, but the π- and non-bonding orbitals of the organic ligand as well. Thus, if the size of a metal framework is mismatched with the "bite-size" of the organic fragment, orbital interaction between the fragments can be improved simply by tilting the terminal hydrogen atoms either away from or closer towards the metal atom(s) [22]. With this in mind, we investigated the effects on metal–ligand

Table 4

Mulliken overlap populations for the interactions of the frontier orbitals of the $[Ru_3(CO)_{10}]^{2-}$ and $[C_3H_5]^+$ fragments

Fragment MO in $[Ru_3(CO)_{10}]^{2-}$	Fragment MO in $[C_3H_5]^+$		
	8 (HOMO)	9 (LUMO)	10
58			0.013
60		0.041	
61			0.037
62		0.135	
63 (HOMO)			0.021
64 (LUMO)	0.087		
65		0.032	
Total MOP per $[C_3H_5]^+$ MO	0.087	0.208	0.071

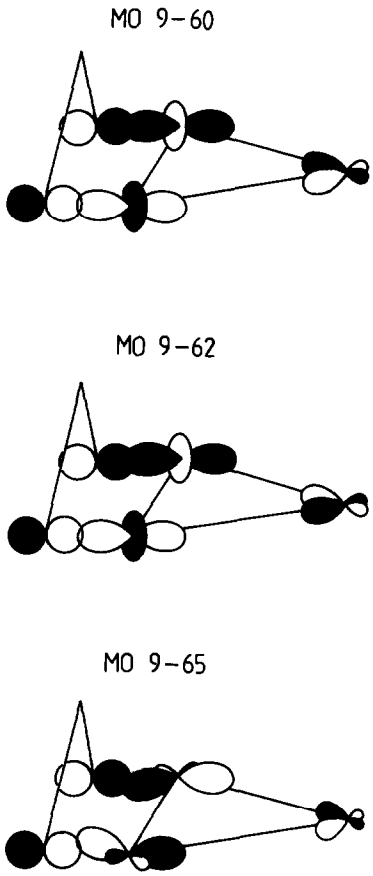

Fig. 4. The major orbital interactions between the fragments $[C_3H_5]^+$ and $[Ru_3(CO)_{10}]^{2-}$.

Table 5

Changes in $[Ru_3(CO)_{10}]^{2-}$ and $[C_3H_5]^+$ fragment MO Mulliken populations upon formation of $[Ru_3(CO)_{10}(C_3H_5)]^-$

$[Ru_3(CO)_{10}]^{2-}$ fragment MO	Orbital population in free ligand (e)	Orbital population in complex (e)	$[C_3H_5]^+$ fragment MO	Orbital population in free ligand (e)	Orbital population in complex (e)
58	2.00	1.96	8 (HOMO)	2.00	1.86
60	2.00	1.77	9 (LUMO)	0.00	1.29
61	2.00	1.77	10	0.00	0.18
62	2.00	0.79			
63 (HOMO)	2.00	1.92			
64 (LUMO)	0.00	0.24			
65	0.00	0.08			

interaction of altering the geometry within the allyl ligand while retaining the experimentally observed carbon atom positions.

Repositioning of the hydrogen atoms in the $[C_3H_5]^+$ ligand was confined to those hydrogens attached to the terminal carbon atoms, C(1) and C(3), since initial investigations had shown that these were the primary points of attachment of the ligand to the metal framework. The hydrogen atom on C(2) remained in a fixed position, coplanar with the CCC skeleton. Each terminal CH_2-unit was rotated about an axis which was parallel to the x-axis (Scheme 1) and which passed through the carbon atom of the CH_2-unit, (Scheme 2) [23*]. As the angle of rotation of each

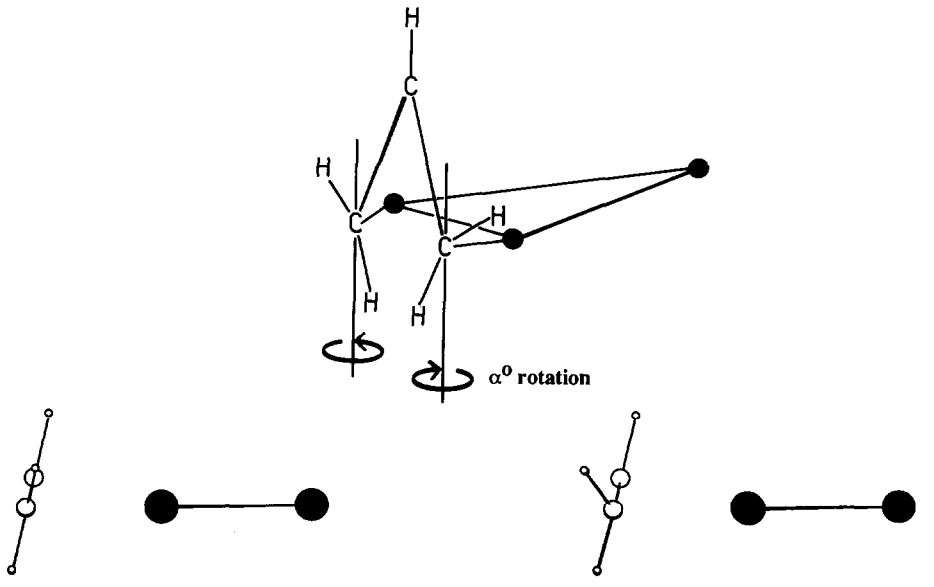

Scheme 2

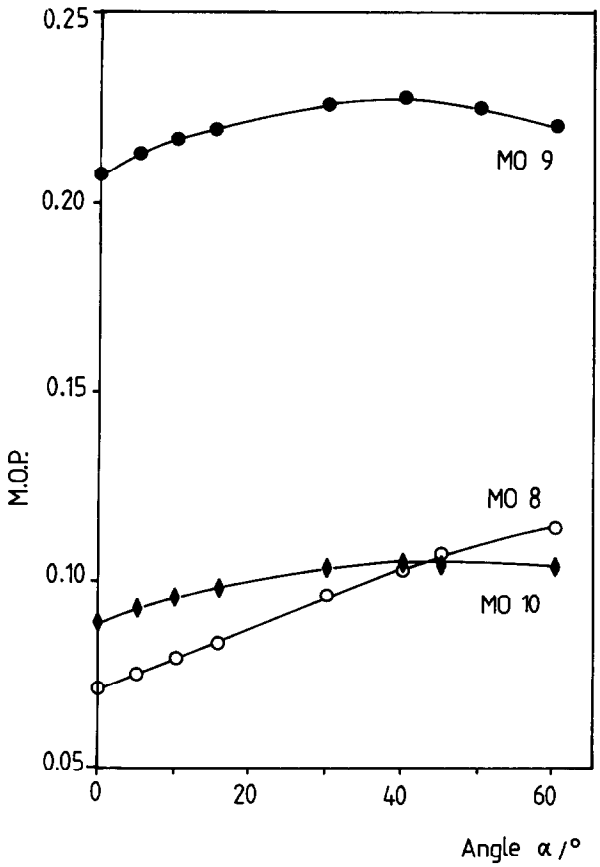

Fig. 5. A plot of the total interfragment Mulliken overlap populations involving MO's 8, 9 and 10 of the allyl ligand as a function of the rotation angle α defined in Scheme 2.

CH_2-unit is increased, the eigenvector contributions to MO's 8, 9, and 10 of the $[C_3H_5]^+$ ligand alter to provide net orbitals which are directed more towards the ruthenium atoms. Figure 5 summarises the changes, and gives the total Mulliken overlap populations as a function of rotation angle for the three primary interaction orbitals of the allyl group with the metal cluster.

A further point to note is that as the terminal hydrogen atoms bend back, rehybridisation at the carbon atoms results in less effective carbon–carbon σ-overlap and a reduction in the degree of delocalisation possible. Thus the intra-allyl bonding is weakened. The final orientation of the hydrogen atoms in the complexed allyl ligand should therefore be such that a balance between maximising metal–ligand bonding without causing too much loss in intra-ligand bonding is struck. Although the calculations do not take into account steric factors, we suggest that it is likely that the hydrogen atoms of the C_3H_5-fragment do bend back away from the trimetal framework. An angle of approximately 30° (Scheme 2 and Fig. 5) results in strong metal–allyl interaction with only a relatively small decrease in intra-allyl bonding. At the same time, the terminal hydrogen atoms do not approach any other atoms too closely.

Interpretation of the ^1H NMR spectrum of 1

The resonances present in the room temperature ^1H NMR spectrum of **1** are listed in Table 2. Numbering of carbon atoms is given in Fig. 1; the *anti/syn* protons on atoms (C(1) and C(3) are labelled as H_a/H_d and H_e/H_b respectively. The multiplet centred at δ 2.69 may be assigned to the unique proton on C(2). Selective decoupling of the remaining sets of resonances at δ 3.42, 3.32, 0.95 and 0.76 allowed the following assignments to be made. The two doublets of doublets of doublets are due to the *syn*-protons, H_b and H_d, each of which is coupled to (i) H_c ($^3J(H_bH_c)$ 5.7, $^3J(H_aH_c)$ 7.4 Hz), (ii) the *anti*-protons H_a and H_e ($^2J(H_bH_a)$ 3.2, $^2J(H_dH_e)$ 2.7 Hz) and (iii) to each other ($^4J(H_bH_d)$ 1.3 Hz). In the majority of cases, coupling of the *syn* and *anti* protons in η^3-allyl ligands is not observed [24], although there is precedence for the observation of a small coupling ($\approx$ 2 Hz) in π-2-chloropalladium complexes [25]. Small, long range (^4J) couplings of inequivalent protons are not uncommon within allyl groups [26]; however, the fact that, in **1**, mutual coupling is observed between the *syn* protons but not between the *anti* protons may be attributed to the former being in a "W" configuration. It follows that the two upfield doublets of doublets can be assigned to the *anti* protons, H_a/H_d. These show a typical *trans*-coupling to H_c ($^3J(H_aH_c)$ 12.3, $^3J(H_eH_c)$ 11.9 Hz) in addition to the geminal coupling to the *syn*-protons described above. This assignment is further corroborated by the observation that *anti*-protons tend to be shifted upfield relative to the *syn*-protons [1a].

Comments on the mechanism involved in the formation of 1

The formation of **1** via the deprotonation of **2** (eq. 1) and the stabilisation of the resultant anion by reaction with Et_3PAuCl deserves comment.

$$HOs_3(CO)_{10}(HC{=}CHMe) \xrightarrow{-H^+} [Os_3(CO)_{10}(H_2CCHCH_2)]^- \quad (1)$$

The allyl anion formally results from the migration of a hydrogen atoms from the methyl group to the C(1) atom. This migration may occur via one of two routes: (i) a direct 1,3-hydrogen shift or (ii) a two-step process involving the triosmium framework. A mechanism similar to (ii) has been proposed for the formation of the η^3-allyl ligand in $Os_3(CO)_8(\mu\text{-}CO)(\eta^3\text{-}CH_2CHCHMe)(\mu\text{-}C(O)NMe_2)$, the sole product in the reaction of $HOs_3(CO)_{10}(\mu\text{-}C(O)NMe_2)$ with $MeC{\equiv}CMe$ [27].

Acknowledgements

C.E.H. wishes to acknowledge the Royal Society for a 1983 University Research Fellowship. The Canadian Government is thanked for support (to J.A.L.)

References

1 See for example (a) M.L.H. Green and P.L.I. Nagy, Adv. Organomet. Chem., 4 (1964) 325; (b) M.A. Bennett, Chem. Rev., 62 (1962) 611; (c) F.A. Cotton and G. Wilkinson, Prog. Inorg. Chem., 1 (1959) 1.

2 (a) C.A. Tolman, J. Am. Chem. Soc., 92 (1970) 6777; (b) C.R. Graham and L.M. Stephenson, J. Am. Chem. Soc., 99 (1977) 7098.

3 A. Cox and P. Woodward, J. Chem. Soc. (A), (1971) 3599.

4 G. Gani, A. Sironi, P. Chini, A. Ceriotti and S. Martinengo, J. Organomet. Chem., 192 (1980) C39.

5 M.I. Bruce and M.L. Williams, J. Organomet. Chem., 288 (1985) C55.

6 B.F.G. Johnson, J.W. Kelland, J. Lewis, A.L. Mann and P.R. Raithby, J. Chem. Soc., Chem. Commun., (1980) 549.
7 M. Evans, M.B. Hursthouse, E.W. Randall, E. Rosenberg and L. Milone, J. Chem. Soc., Chem. Commun., (1972) 545.
8 F.G. Mann, A.F. Wells and D. Purdie, J. Chem. Soc., (1937) 1828.
9 C.R. Eady, B.F.G. Johnson, J. Lewis and M.C. Malatesta, J. Chem. Soc., Dalton Trans., (1978) 1358.
10 Obtained as a minor product in the reaction of $H_2Os_3(CO)_{10}$ with MeC_2H: A.J. Deeming, S. Hasso and M. Underhill, J. Chem. Soc., Dalton Trans., (1975) 1614.
11 $HOs_3(CO)_{10}(HCCHMe)$ (**2**) can be synthesised in ca. 50–60% yield by the reaction of $[PPN][HOs_3(CO)_{11}]$ with MeC_2H followed by protonation by HBF_4.
12 SHELXTL76, Crystal Structure Determination Package, G.M. Sheldrick, Cambridge, 1976.
13 International Tables for X-ray Crystallography, Kynoch Press, Birmingham, 1974, vol. 4.
14 M.B. Hall and R.F. Fenske, Inorg. Chem., 11 (1972) 768.
15 The validy of PH_3 as a model phosphine in Fenkse–Hall calculations has been tested: N.M. Kostic and R.F. Fenske, Organometallics, 1 (1982) 489.
16 E. Clementi, J. Chem. Phys., 40 (1964) 1944.
17 J.W. Richardson, M.J. Blackman and J.F. Ranochak, J. Chem. Phys., 58 (1973) 3010.
18 G. Lavigne, F. Papageorgiou and J.-J. Bonnet, Inorg. Chem., 23 (1984) 609.
19 (a) D.G. Evans and D.M.P. Mingos, J. Organomet. Chem., 232 (1982) 171; (b) D.M.P. Mingos, J. Chem. Soc., Dalton Trans., (1976) 1163; (c) K.P. Hall and D.M.P. Mingos, Prog. Inorg. Chem., 32 (1984) 237.
20 C.E. Housecroft and A.L. Rheingold, Organometallics, 6 (1987) 1332.
21 B.E.R. Schilling, R. Hoffmann, and J.W. Faller, J. Am. Chem. Soc., 101 (1979) 592.
22 M. Elian, M.M.L. Chien, D.M.P. Mingos and R. Hoffmann, Inorg. Chem., 15 (1976) 1148.
23 Rotation about other axes lessened rather than optimised ligand to metal bonding.
24 H.S. Gutowsky, M. Karplus and D.M. Grant, J. Chem. Phys., 31 (1959) 1278.
25 M.S. Lupin and B.L. Shaw, Tetrahedron Lett., (1964) 883.
26 D.H. Williams and I. Fleming, Spectroscopic Methods in Organic Chemistry, 3rd ed., McGraw-Hill, London, 1980, p. 108.
27 H.D. Kaesz, W. Krone-Schmidt, W.J. Sieber, N.M. Boag and C.B. Knobler, Proc. 5th International Symposium on Relations between Homogeneous and Heterogeneous Catalysis, 1986.